Nanoscale Mapping of the Conductivity and Interfacial Capacitance of an Electrolyte Gated Organic Field Effect Transistor under Operation

Adrica Kyndiah[*]*, Martí Checa, Francesca Leonardi, Ruben Millan-Solsona, Martina Di Muzio, Shubham Tanwar, Laura Fumagalli, Marta Mas-Torrent, Gabriel Gomila*[*]

Dr. A. Kyndiah, Dr. M. Checa, R. Millan-Solsona, M. Di Muzio, S. Tanwar, Prof. G.Gomila
Nanoscale Bioelectrical Characterization Group,
Institute for Bioengineering of Catalonia (IBEC),
The Barcelona Institute of Science and Technology (BIST),
Carrer Baldiri i Reixac 11-15,
08028 Barcelona, Spain
E-mail: akyndiah@ibecbarcelona.eu, ggomila@ibecbarcelona.eu

Dr. A. Kyndiah, R. Millan-Solsona, Prof. G. Gomila
Departament d'Enginyeria Electrònica i Biomèdica,
Universitat de Barcelona,
C/ Martí i Franquès 1,
08028 Barcelona, Spain

Dr. F. Leonardi, Dr. M. Mas-Torrent
Institut de Ciència de Materials de Barcelona (ICMAB-CSIC) and Networking Research Centre on Bioengineering Biomaterials and Nanomedicine (CIBER-BBN)
Campus UAB Cerdanyola del Vallès,
08193 Barcelona, Spain

[+]Present Address
Dr. Francesca Leonardi
OnePlanet Research Center
Wageningen Campus
Impulse (building 115), Stippeneng 2
6708WE
Wageningen
The Netherlands

Dr. L. Fumagalli
Department of Physics and Astronomy and National Graphene Institute
The University of Manchester,
Manchester M13 9PL, United Kingdom.

Keywords: Electrolyte Gated Organic Field Effect Transistor (EGOFET), In-liquid Scanning Dielectric Microscopy (In-liquid SDM), Organic semiconducting blend, Atomic Force Microscopy (AFM), Bioelectronic devices

Probing nanoscale electrical properties of organic semiconducting materials at the interface with an electrolyte solution under external applied voltages is key in the field of organic

bioelectronics. It is demonstrated that the conductivity and interfacial capacitance of the active channel of an Electrolyte Gated Organic Field Effect Transistor (EGOFET) under operation can be probed at the nanoscale using Scanning Dielectric Microscopy in force detection mode in liquid environment. Local electrostatic force vs gate voltage transfer characteristics at each point on the device are obtained and correlated with the global current-voltage transfer characteristics of the EGOFET. The nanoscale maps of the conductivity of the semiconducting channel shows the dependence of the channel conductivity on the gate voltage and its variation along the channel due to the space charge limited conduction. The maps reveal very small electrical heterogeneities, which correspond to local interfacial capacitance variations due to an ultrathin non-uniform insulating layer resulting from a phase separation in the organic semiconducting blend. Present results offer insights on the transduction mechanism at the organic semiconductor/electrolyte interfaces at scales down to ~100nm, which can bring substantial optimization of organic electronic devices for bioelectronic applications such as electrical recording on excitable cells or label-free biosensing.

1. Introduction

In recent years the field of organic bioelectronics has experienced a fast evolution and development, with relevant emerging bioelectronic applications, among which the realization of bioelectronic recordings in excitable cells[1–3] and the development of label-free biosensors.[4–8] One of the main devices used in these applications are the Electrolyte Gated Organic Field Effect Transistors (EGOFETs). EGOFETs are based on organic semiconductors that are normally non-permeable to ions, and whose free carrier density is modulated by the electric field generated at the semiconductor/electrolyte interface.[9–11] The deposited organic semiconducting layers, which are vacuum sublimed or solution processed, have a nanostructured nature either due to its poly-crystallinity or due to the presence of different phases and components. Device characterization and optimization, then, requires the use of

nanoscale electrical characterization techniques, typically based on scanning probe microscopies, as it is done for organic devices operated in air.[12,13] EGOFETs, however, have the organic semiconducting film in contact with an electrolyte solution. This configuration complicates severely the possibility to probe the local electric properties (e.g. potential, free carrier density, conductivity or interfacial capacitance) of the charge transporting layer of the devices *in operando*, due to the lack of nanoscale electrical characterization techniques able to operate in electrolyte solutions. For instance, Kelvin Probe Force Microscopy (KPFM), widely used to map the electric potential distribution and charge trapping dynamics[14,15] in functional organic transistors operated in air or vacuum,[12,13,16,17] still has not been demonstrated for transistors operated in electrolyte solutions. On the other hand, Electrochemical Strain Microscopy (ESM) has shown the possibility to probe local variations in ion transport in Organic Electrochemical Transistors (OECTs) from the measurement of sub-nanometre volumetric expansions due to ion uptake.[18] However, this technique does not provide relevant information when applied to organic semiconductors in which ion uptake does not take place, as in most EGOFETs. Finally, microscale local potential measurements by Scanning Electrochemical Microscopy have been demonstrated also on OECTs[19], but they are based on the good conducting properties of OECTs, which are not generally met in EGOFETs.

Therefore, techniques that can directly probe the nanoscale electrical properties of the organic semiconducting channel in contact with the electrolyte solution in an EGOFET during device operation are still lacking. Establishing them would offer new insights into the physicochemical electrical transduction mechanisms at the organic semiconductor/electrolyte interfaces and would pave the way for the optimization of these, and other, organic devices for bioelectronic applications.

In the present study, we focus on mapping the local electrical conductivity of EGOFETs in operando. The conductivity is given by (see also **Supporting Information S1**)

$$\sigma(x) = e\mu n(x) \quad (1)$$

where *e* is the electron charge, μ is the carrier mobility along the in-plane direction and n(x) the free carrier concentration in the organic semiconductor film averaged along the transversal direction. The carrier concentration, n(x), can be determined by assuming the semiconductor forms the plate of a capacitor[20] so that (see also Supporting Information S1)

$$en(x)h = c_{\text{int,s}}(x)\left[V(x) - V_{sol}(x)\right] \quad (2)$$

where $c_{int,s}$ (x) is the capacitance per unit of area of the semiconductor/electrolyte interface, h the film thickness and V(x) (res. V_{sol}(x)) the electric potential in the semiconductor channel (res. electrolyte) with respect to the source at position *x* along the semiconducting channel of the EGOFET.

The mapping of the conductivity then can reveal spatial variations of the free carrier concentration due to variations of the voltage along the channel due to the space charge limited transport and to local variations in the semiconductor/electrolyte interfacial capacitance , which are not accessible from the analysis of the transfer I_{DS}-V_{GS} or output I_{DS}-V_{DS} characteristics that normally provide averaged information (see **Supporting Information S2**).

To map the local conductivity of an EGOFET channel under operation in an electrolyte solution, we employed in-liquid Scanning Dielectric Microscopy (in-liquid SDM). SDM is a scanning probe microscopy technique that can be applied in either current[21,22] or force-sensing [23–25] to obtain high spatial resolution electric and dielectric functional maps of materials in air[22,23] and in liquid environment[24–26] (see **Supporting information S3**).

As an example of application we consider EGOFETs based on a blend of the organic semiconducting material 2,8-Difluoro-5,11-bis(triethylsilylethynyl)anthradithiophene (diF-TES-ADT) with the insulating polymer polystyrene (PS), which we recently used as a bioelectronic recording platform for excitable cells.[3,27] EGOFETs based on organic blends have attracted the attention during the past few years due to their enhanced electrical

performance and remarkable stability.[28,29] The impressive performance of these devices is believed to be correlated to the nanoscale structure of the organic semiconductor thin film, which shows an enhanced crystallinity and, in some cases, the presence of a nanostructured top insulating protective layer derived from a vertical phase separation phenomenon. [30–32]

2. Results and Discussion

The set-up implemented to carry out the *in-operando* nanoscale electrical measurements is shown schematically in **Figure 1.** In it the metallic (platinum coated) cantilever probe is used as both gate electrode for the EGOFET transistor and as a recording force sensor for the in-liquid SDM measurements. A DC+AC amplitude modulated voltage

$$V_{probe}(t) = V_{GS} + \frac{V_{ac}}{2}\left(1 + cos(\omega_{mod}t)\right)\cos(\omega_{el}t) \quad (3)$$

is applied to the probe (gate) with respect to the source electrode. The AC part of the voltage is used to generate and detect a cantilever oscillation harmonic at ω_{mod} that is sensitive to only the local AC polarization properties of the sample at the frequency ω_{el}[24]. The angular frequency ω_{el} is in the MHz range, beyond both the dielectric relaxation frequency of the electrolyte and the mechanical resonance frequency of the cantilever. The free carrier concentration in the semiconductor channel of the EGOFET is practically not modulated by the high frequency voltages used in SDM due to the poor coupling of the electrolyte with the channel at these frequencies (see **Supporting Information S4**). As a result, SDM measurements are not sensitive to the semiconductor channel capacitance as in C-V measurements [27] but to the (local) conductivity of the organic semiconductor thin film and the (local) interfacial capacitance of the semiconductor/electrolyte interface (see **Supporting Information S5**). We note that, on the devices studied here, ~~due to the tip-device geometry~~ SDM is sensitive to the conductivities along and transversal to the channel. The DC voltage applied to the probe is used as a gate voltage V_{GS} to polarise the transistor. The electric current flowing in the device, in response to the source drain voltage V_{DS}, is measured in real time with

a current-voltage source meter connected to the device while *in situ* in-liquid SDM measurements are performed on the EGOFET.

The EGOFETs based on the organic semiconducting blend composed of diF-TES-ADT and PS were fabricated by using the Bar Assisted Meniscus Shearing technique BAMS as described earlier[33]. The active organic semiconducting layer is separated from the gate electrode by an aqueous electrolyte, which in our case was Milli-Q water. Current-voltage transfer characteristics of the EGOFET using the probe as gate electrode have been measured and show the classical response of an EGOFET that work in accumulation mode in deionised water (see **Supporting information S6 and S7**).

In-liquid SDM measurements on the EGOFET *in operando* were performed by operating the technique in the so-called force volume mode (see Supporting Information S3), recently introduced in air environment.[34] We analysed an area of the transistor which comprises the Source-Channel-Drain, as shown by the AFM topographic image in **Figure 2a**. The channel length is around 30 μm and presents some clearly visible nanoscale morphological heterogeneities, including some holes in the semiconductor layer (from where the thickness of the organic thin film layer was estimated to be 20-30 nm). The electrodes are about 50 nm thick (see cross-section topographic profile in **Figure 2b** taken along the dashed line in Figure 2a). Representative AC electric force-distance curves taken at a pixel located at the centre of the channel at different gate voltages V_{GS} are shown in **Figure 2c**. The force is represented through the capacitance gradient *dC/dz* [aF/nm], which is related to the force by $F_{\omega mod}=1/8\ dC/dz\ v_{ac}^2$ [35].

The *dC/dz* curves show a dependence of the electric force on the tip-sample distance, which is a sign of the locality of the measurement. The most relevant feature shown by the curves is that they shift up and change its "concavity" when the gate voltage, V_{GS}, is sweep from 0 V to –0.6 V. Variations of the electric force with distance are more pronounced when the gate voltage

surpasses the voltage $V_{GS} \sim -0.2$ V, which coincides with the threshold voltage of the transistor (as measured from the current-voltage transfer characteristics in Supporting Information S6). The changes observed in the AC electric force-distance curves as a function of the gate voltage can be directly attributed to a change in the effective (local) conductivity of the semiconducting channel due to the variation of the gate voltage, see Supporting Information S5. Note that the active material is a p-type semiconductor that works in accumulation mode, and an increase in the hole charge carrier density is expected with more negative gate voltages. The dependence of the electric force on conductivity can be qualitatively explained as follows. When the transistor is in the off-state the carrier concentration density in the channel is very low, and the AC electric field inside it is little screened out (the channel behaves like an insulator with losses). As a result, most of the AC voltage applied to the tip drops in the semiconductor layer (which has a relatively small relative permittivity $\varepsilon_{sem} \sim 4$), and on SiO_2 substrate (which also has a low relative permittivity $\varepsilon_{SiO2} \sim 4$), and very little in the electrolyte solution (which has a large relative permittivity, $\varepsilon_{sol} \sim 78$), resulting in a low AC electric force acting on the tip (black, red and blue curves of Figure 2c). When the transistor passes to the on-state the carrier concentration in the channel increases rapidly. Consequently, the AC electric field inside the semiconductor layer gets strongly screened and very little AC potential drops in it. Therefore, most of the AC potential drops in the electrolyte solution between the tip and the semiconductor layer, resulting in a large AC force acting on the tip, which shows a sharp increase at the closest distances. These results show that the force distance curves obtained by in-liquid SDM are sensitive to (local) changes in the conductivity of the organic semiconductor film in contact with the electrolyte solution under *in operando* conditions (see Supporting Information S5 for further details). We have quantified the local conductivity of the semiconductor channel as a function of the gate voltage by using the methods of SDM [23,24] (dashed lines in Figure 2c, see Supporting Information S3). The extracted conductivity as a function of V_{GS} is shown by the

green curve in **Figure 2d**. When the transistor undergoes the transition from the off to the on-state, the local conductivity increases sharply with the gate voltage V_{GS}, followed by an almost linear dependence on it. The qualitative behaviour of the local conductivity as a function of the gate voltage is similar to the global conductivity obtained from the analysis of the I-V characteristics (see Supporting Information S2). Quantitatively the values can be somewhat higher due to different effects (e.g. field dependent mobility, contact resistance effects or sensitivity to the interfacial capacitance) as discussed in the **Supporting Information S8**.

From the electric force-distance curves acquired at different gate voltages one can derive local electric force-voltage device transfer characteristics and correlate them with the conventional current-voltage transfer characteristics of the EGOFET. In Figure 2d we plot on the left axis, in log-linear scale, the source-drain current I_{SD} versus gate-source voltage V_{GS} measured from the transistor with the current-source meter during the in-liquid SDM measurements. On the right axis, in linear-linear scale, we plot the capacitance gradient (force) measured at the centre of the channel by the in-liquid SDM set-up as a function of the gate voltage V_{GS} (bottom x-axis) at a given tip sample distance (in this case Z=180 nm with respect to the semiconductor surface, see **Supporting Information S9** for electric force transfer characteristics at different heights). In this graphical representation, there is a direct overlap between the global current-gate voltage transfer characteristics and the local electrostatic force-gate voltage transfer curve, demonstrating that both types of transfer curves provide similar information. The above results fit well with what one would expect in an OFET and thus confirms that in-liquid SDM measurements probe the change in the local conductivity of the channel during the EGOFET operation.

The previous analysis, which has been performed at a single point in the channel, can be performed in all points of the device (source, drain and channel). We show the corresponding set of force-gate voltage curves at a distance Z=180 nm with respect to the surface of the

semiconductor in the inset of Figure 2d. We have plotted in different colours the local force-voltage transfer characteristics in the channel (blue), source (black) and drain (red). In absolute values the forces on the source and drain are higher than on the channel, since the source and drain parts of the transistor are closer to the tip at the chosen distance at which the transfer curves have been extracted, and also because the substrate underneath the semiconductor is an electrode instead of an insulator (see Supporting Information S5). Some variability exists in the electric force transfer characteristics obtained at the different points in the channel (and on the source and drain regions), which reflect slightly different local electrical properties. This spatial variability can be better illustrated by building up constant height electric force images for the different gate voltages. These images are obtained from the local electric force-voltage transfer curves by selecting the values corresponding to a given gate voltage at the selected tip-sample distance.[34] **Figure 3a** shows examples of electric images obtained for a tip-channel distance Z=180 nm with respect to the surface of the semiconductor (electric images for different Z can be found in **Supporting Information S10**) and for gate voltages V_{GS} from 0 V to −0.6 V. Concerning the semiconductor channel, when the gate voltage is below the threshold voltage (off state) it shows an almost uniform and symmetric distribution of the electric forces (except for edge effects), which is independent from the gate voltage (see black, red and blue central average cross-section profiles in **Figure 3b**).When the gate voltage passes the threshold voltage (V_{GS}<−0.2 V), we observe a change in the contrast of the electric images, which reflects an increase in the force acting on the tip in all parts of the device. We note that the electric forces are larger on the source than on the drain (see **Figure 3c)**. This fact is due to the presence of a non-zero source drain voltage V_{DS} that makes that the conductivity in the source and drain are different (for V_{DS}=0 V the forces are similar in both the source and drain, see **Supporting Information S11**). In the channel, we also see the gradual decrease of the force from the source to the drain for the same reason. Repeating at each pixel the analysis done at the center of the

channel in Figure 2c, we have calculated conductivity maps for the central part of the channel for different gate voltages (see Figure 3c). **Figure 3d** shows averaged conductivity profiles along the channel obtained from each image. The conductivity in the channel changes both globally, because of the gate voltage, and along the channel on a large scale (micrometres) due to the source drain voltage. This result implies that the conductivity of the channel can be mapped from in-liquid SDM measurements.

Finally, spatial heterogeneities at small scales (sub-micrometric) are also observed in the force and conductivity images of the channel for gate voltages above the threshold voltage. Some heterogeneities can be simply correlated to the sample morphology. For instance, in the upper right corner of the channel there appears an electrical heterogeneity in the force image (Figure 3a) due to a hole in the semiconductor layer (see Figure 2a). Some other heterogeneities observed, however, are not so simply correlated with the semiconductor morphology, e.g. those observed in the central part of the channel (see Figures 3a and 3c). A possible source of these small scale conductivity heterogeneities could be attributed to variations in the interfacial capacitance. Indeed, the conductivity images have been built by assuming a uniform interfacial capacitance for the semicoductor/electrolyte interface, whose value was determined from measurements performed on the source (see Supporting Information S5). If the actual interfacial capacitance is not uniform, its variations from point to point will be translated into variations into the extracted conductivity vales (see **Supporting Information S12**). This suggests that the surface of the transistor channel shows a nanoscale heterogeneous composition. The origin of such an heterogenous composition could be the same as that reported for another semiconductor blend containing 2,7-Dioctyl[1]benzothieno[3,2-b][1]benzothiophene and polystyrene (C8-BTBT:PS)[30], for which it was reported that a vertical phase separation occurred in which the organic semiconductor is sandwiched between a bottom PS layer and another top non-uniform ultrathin PS layers ~0.5–2 nm thick. In

electrical terms, the presence of a local ultrathin insulating layer would introduce a local interfacial capacitance variation, $c_{int,s}(x)$, to which the in-liquid SDM measurements are also very sensitive, as shown in [25] and also shown here in the Supporting Information S5 and as discussed elsewhere for the case of nanopatterned Self-Assembled-Monolayers SAM at metal/electrolyte interfaces.[35] The presence of an insulating layer of low dielectric constant (like PS, ε_{PS}~2) on top of the semiconducting material induces a voltage drop on the layer which is larger than on the sourrounding aqueous solution (which has a much higher dielectric constant, ε_{sol}~78). Therefore, the force acting on the tip when on top of the ultrathin insulating layer is expected to be smaller than when on the bare semiconductor. Consequently, the regions showing smaller forces are expected to correspond to those with the presence of the ultrathin PS layers. In terms of the extracted conductivities (Figutre 3c), if the model assumes a uniform interfacial capacitance, force reductions due to a reduction of the interfacial capacitance will be translated into a decrease of the extracted conductivity (see Supporting Information S12). To further confirm this interpretation we have acquired additional electrical and AFM images (topography, adhesion and mechanical phase). The results of some representative regions of the channel are shown in **Figure 4**. In (a)-(c) we show topography, adhesion and electric force images, respectively, obtained from a single set of SDM measurements on the selected region. In (d) and (e) we show intermittent contact topography and phase images of another region, respectively, and the corresponding in-liquid SDM constant height electric force image in (f). Both electrical images (c) and (f) correspond to Z=30 nm from the surface of the semiconductor with the transistor in the on state (V_{GS}= –0.5 V for the case of **Figure 4c** and V_{GS}= –0.3 V for **Figure 4f**). V_{DS} is always kept at –0.5 V. We observe that when abrupt decreases in the force are observed in the electric images on top of the smooth variation along the channel, either the adhesion or the mechanical phase in the AFM images also present some abrupt variations (in the topographic images sometimes a small variation below ~1 nm can be also observed). The

fact that the electric force decreases on the heterogeneity indicates that it corresponds to a region covered by the (ultrathin) insulating layer. These results confirm that the heterogeneities observed in the force and conductivity images correspond to variations of the local interfacial capacitance of the semiconductor/electrolyte interface caused by the presence of an heterogeneous distribution of an ultrathin PS layer on top of the organic semiconductor. We have estimated a variation of interfacial capacitance in this case from ~1.3 $\mu F/cm^2$ to ~0.3 $\mu F/cm^2$ when passing from the semiconductor to the PS coated part (see **Supporting Information S13**). It should be noted that these heterogeinities resulting from the blend do not hinder the overall performance of the EGOFET. The addition of PS enhances the material processability resulting in more crystalline films and stable devices as compared to the ones based on only the semiconductor.[27] The stability of these EGOFETs could be partly related to the observed ultra thin layer of PS that could act as a capping layer to ion diffusion into the semiconductor[36]. Having access to this information can be specifically useful for the case of biosensors based on organic transistors and to better understand the coupling of excitable cells with these devices for electrical cell recordings.[3]

The application of the present approach to other electrolyte gated transistors, including Organic Electrochemical Transistors (OECTs), requires further study. OECTs do not have a field-effect transport but rather an ionic modulation of a high bulk conductivity. SDM can be sensitive to high conductivity variations, but higher frequencies, probably in GHz range would be required. Similarly, measurements in electrolytes at higher ionic concentrations (beyond 100 mM) would also require the use of frequencies in the GHz range[24]. Detection of GHz signals with force detection methods has been shown in the analysis of microwave integrated circuits[37]. Properly adapted, it could also be done for the in-liquid SDM measurements reported here. Concerning the spatial resolution and acquisition times, we expect that sub-100

nm and sub-30 sec images could be obtained on EGOFETs with the use of high resonance frequency probes.[34,35]

3.Conclusion

To conclude, in this work we applied in-liquid Scanning Dielectric Microscopy to study the nanoscale electrical properties (conductivity and interfacial capacitance) of a fully functional Electrolyte Gated Organic Field Effect Transistor. We have first shown that the AC electric force vs distance approach curves measured at single points in the channel are sensitive to the local conductivity, i.e. to the free hole carriers concentration. Thanks to this sensitivity, local electric force-voltage transfer characteristics can be obtained at all points in the channel, which nicely correlate with the global device current-voltage transfer characteristics. Conductivity maps of the transistor channel reveal both global conductivity variations due to changes in the gate voltage and variations along the channel due to the space charge conduction in an accumulation mode field effect transistor. The conductivity maps have also revealed minute heterogeneities at small scales (micron and sub-micron) that we have correlated to variations of the interfacial capacitance of the semiconductor/electrolyte interface. For the semiconductor blend diF-TES-ADT:PS used in the EGOFETs analyzed here, these result show that a vertical phase separation takes place with the PS forming heterogeneous ultrathin layers on top of the semiconductor material.The electrical images enable to directly identify which parts of the surface are covered by PS and which parts are not and to quantify the local variations in the interfacial capacitance. Such findings would offer the possibility to optimize the device performance such as increasing the coverage of the ultra thin PS layer to enhance stability or eliminate this layer in order to have a better coupling at the semiconductor/electrolyte interface. The results presented open fascinating possibilities to study the transduction mechanisms at the organic semiconductor/electrolyte interface relevant

for electrolyte gated transistors and to optimize device fabrication and performance for bioelectronic applications.

4. Experimental Section

Device fabrication

A heavily doped n-type silicon wafer featuring thermal SiOx (200 nm thick) was used as substrate for our devices into which source and drain (S/D) electrodes were defined by photolithography as described earlier[3,27]. The channel width (W) and length (L) were 19680 μm and 30 μm respectively. Prior to the deposition of the organic semiconductor, the substrates were cleaned in ultrasonic bath with acetone and isopropanol for 15 min respectively and afterward ozone-treated for 25 min. S/D electrodes were subsequently modified by immersing the device in a 15 mM pentafluorothiophenol (PFBT) solution in isopropanol for 15 minutes. A blend composed of diF-TES ADT and polystyrene (PS) was mixed in a 4:1 ratio, and then dissolved in chlorobenzene reaching a final concentration of 2 wt%. The blend solution was kept on a hot plate at 105 °C for 1 h to ensure the complete dissolution of the starting materials. Thin film deposition was realized through Bar-Assisted Meniscus Shearing (BAMS) technique by means of a home-adapted bar coater working at fixed speed of 1 cm s^{-1} and at a fixed plate temperature of 105 °C as reported earlier. [27,31] All the above-mentioned processes were realized under ambient conditions.

In-liquid Scanning Dielectric Microscopy on functional EGOFET

SDM measurements have been performed in liquid following approaches presented earlier[24,25]. In a nutshell, an amplitude modulated AC voltage (Eq. (1)) of amplitude 1.5 V_{PP}, electrical frequency in the range 1–10MHz and modulating frequency of 2kHz has been applied by means of a function generator (33220A Function Waveform Generator, Keysight) between the conductive probe of an AFM system and the source electrode of the EGOFET. In order to polarise the transistor, a V_{DC} offset (equivalent to the gate-source voltage V_{GS}) is applied in

addition to the AC voltage driving the tip's movement. A constant voltage V_{DS} is applied externally using the Source Measuring Unit Agilent 2912B. The ground of all the equipments have been short circuited in order not to have floating potentials. The so-called force volume mode has been used to acquire the data, as described in the text and previsouly applied in air[34]. Normal deflection and $A_{\omega mod}$ oscillation amplitude approach curves were acquired using the JPK Nanowizard 4 AFM system (JPK) connected to an external lock-in (eLockin 204/2, Anfatec). The acquisition was performed by using the Advanced Quantitative Imaging (JPK) mode. The set of SDM data of Figure 3a consisted of 64 X 13 deflection and ω_{mod}-oscillation amplitude approach curves, each one with 300 data points and spanning a length of about 2.5 μm. The SDM data of Figures 4c consisted of 128 X 26 pixels and that of figure 4f consisted of 128 X 23 pixels. The acquisition time per pixel was 300ms, and the lock-in integration time was set to 2 ms, with a gain $G_{lock\text{-}in}$=50. The measurements have been carried out by using PPP-CONTPt tips (NANOSENSORS), with equivalent spring constant k=1.2N/m and resonance frequency in liquid of around 11KHz. To acquire an image of 65x13 pixels it took around four minutes per set of SDM data for each gate voltage. Electrical oscillation amplidudes are converted to electric forces as detailed elsewhere.[23],[35]

Quantitative analysis

Numerical calculations were used to relate the electric force acting on the tip to the local conductivity and interfacial capacitance of the organic semiconductor. The numerical calculations have been implemented in COMSOL Multiphysics 5.4 linked to a custom made Matlab interface using the modelling developed earlier in Refs [23,24,38,39] adapted here to include tip interfacial capacitance effects, as detailed elsewhere Ref [35] and to deal with conductive samples. Further details are provided in the Supporting Information S3 and S5.

Supporting Information

Supporting Information is available from the Wiley Online Library or from the author.

Acknowledgements

This work has been partially supported by the BEST Postdoctoral Programme funded by the European Commission under Horizon 2020's Marie Curie Sklodowska-Curie Actions COFUND scheme (GA 712754) and the Severo Ochoa programme of the Spanish Ministry of Science and Competitiveness (SEV-2014-0425), the BORGES project (Marie Curie Skłodowska European Training Network (MSCA-ITN-ETN)) under the Grant Agreement (GA 813863), and the Agencia Estatal de Investigacion (Nanoelectrophys project, TEC2016-79156-P). Support from an ICREA Academia award (G.G), the 2017-SGR1079 grant and the CERCA program from the Generalitat de Catalunya is also acknowledged. F.L and M.M-T were funded by the Spanish Ministry (project FANCY CTQ2016-80030-R), the Generalitat de Catalunya (2017-SGR-918) and the Spanish Ministry of Economy and Competitiveness, through the "Severo Ochoa" Programme for Centers of Excellence in R&D (SEV-2015-0496). F.L acknowledges the *Juan de la Cierva* fellowship. The authors also thank the Networking Research Center on Bioengineering, Biomaterials, and Nanomedicine (CIBER-BBN). L. F. received funding from the European Research Council (grant agreement No. 819417) under the European Union's Horizon 2020 research and innovation programme. The authors would like to thank Prof. T. Cramer for the measurement software of the EGOFETs and for scientific discussion.

Received: ((will be filled in by the editorial staff))
Revised: ((will be filled in by the editorial staff))
Published online: ((will be filled in by the editorial staff))

References

[1] D. Khodagholy, T. Doublet, P. Quilichini, M. Gurfinkel, P. Leleux, A. Ghestem, E. Ismailova, T. Hervé, S. Sanaur, C. Bernard, G. G. Malliaras, *Nat. Commun.* **2013**, *4*.

[2] T. Cramer, B. Chelli, M. Murgia, M. Barbalinardo, E. Bystrenova, D. M. de Leeuw, F. Biscarini, *Phys. Chem. Chem. Phys.* **2013**, *15*, 3897.

[3] A. Kyndiah, F. Leonardi, C. Tarantino, T. Cramer, R. Millan-Solsona, E. Garreta, N. Montserrat, M. Mas-Torrent, G. Gomila, *Biosens. Bioelectron.* **2020**, *150*, 111844.

[4] S. Casalini, F. Leonardi, T. Cramer, F. Biscarini, *Org. Electron. physics, Mater. Appl.* **2013**, *14*, 156.

[5] E. Macchia, K. Manoli, B. Holzer, C. Di Franco, M. Ghittorelli, F. Torricelli, D. Alberga, G. F. Mangiatordi, G. Palazzo, G. Scamarcio, L. Torsi, *Nat. Commun.* **2018**, *9*.

[6] R. A. Picca, K. Manoli, E. Macchia, L. Sarcina, C. Di Franco, N. Cioffi, D. Blasi, R. Österbacka, F. Torricelli, G. Scamarcio, *Adv. Funct. Mater.* **2019**, *1904513*, 1.

[7] M. Berto, C. Diacci, R. D'Agata, M. Pinti, E. Bianchini, M. Di Lauro, S. Casalini, A. Cossarizza, M. Berggren, D. Simon, G. Spoto, F. Biscarini, C. A. Bortolotti, *Adv. Biosyst.* **2018**, *2*, 1.

[8] C. Diacci, M. Berto, M. Di Lauro, E. Bianchini, M. Pinti, D. T. Simon, F. Biscarini, C. A. Bortolotti, *Biointerphases* **2017**, *12*, 05F401.

[9] L. Kergoat, L. Herlogsson, D. Braga, B. Piro, M. C. Pham, X. Crispin, M. Berggren, G. Horowitz, *Adv. Mater.* **2010**, *22*, 2565.

[10] T. Cramer, A. Kyndiah, M. Murgia, F. Leonardi, S. Casalini, F. Biscarini, *Appl. Phys. Lett.* **2012**, *100*, 143302.

[11] T. Cramer, A. Campana, F. Leonardi, S. Casalini, A. Kyndiah, M. Murgia, F. Biscarini, *J. Mater. Chem. B* **2013**, *1*, 3728.

[12] P. Annibale, C. Albonetti, P. Stoliar, F. Biscarini, *J. Phys. Chem. A* **2007**, *111*, 12854.

[13] K. P. Puntambekar, P. V. Pesavento, C. D. Frisbie, *Appl. Phys. Lett.* **2003**, *83*, 5539.

[14] T. Hallam, M. Lee, N. Zhao, I. Nandhakumar, M. Kemerink, M. Heeney, I. McCulloch, H. Sirringhaus, *Phys. Rev. Lett.* **2009**, *103*, 1.

[15] P. A. Bobbert, A. Sharma, S. G. J. Mathijssen, M. Kemerink, D. M. De Leeuw, *Adv. Mater.* **2012**, *24*, 1146.

[16] V. Palermo, M. Palma, P. Samori, *Adv. Mater.* **2006**, *18*, 145.

[17] L. S. C. Pingree, O. G. Reid, D. S. Ginger, *Adv. Mater.* **2009**, *21*, 19.

[18] R. Giridharagopal, L. . Flagg, J. . Harrison, M. . Ziffer, J. Onorato, C. . Luscombe, D. . Ginger, *Nat. Mater.* **2017**, *16*, 1.

[19] F. Mariani, F. Conzuelo, T. Cramer, I. Gualandi, L. Possanzini, M. Tessarolo, B. Fraboni, W. Schuhmann, E. Scavetta, *Small* **2019**, *1902534*, 1.

[20] S. M. Sze, W. SHOCKLEY, *Proc. I.R.E* **1952**, *40*, 473.

[21] L. Fumagalli, G. Ferrari, M. Sampietro, G. Gomila, *Appl. Phys. Lett.* **2007**, *91*.

[22] L. Fumagalli, G. Ferrari, M. Sampietro, G. Gomila, *Nano Lett.* **2009**, *9*, 1604.

[23] L. Fumagalli, D. Esteban-Ferrer, A. Cuervo, J. L. Carrascosa, G. Gomila, *Nat. Mater.* **2012**, *11*, 808.

[24] G. Gramse, M. A. Edwards, L. Fumagalli, G. Gomila, *Appl. Phys. Lett.* **2012**, *101*, 213108.

[25] L. Fumagalli, A. Esfandiar, R. Fabregas, S. Hu, P. Ares, A. Janardanan, Q. Yang, B. Radha, T. Taniguchi, K. Watanabe, G. Gomila, K. S. Novoselov, A. K. Geim, *Science (80-.).* **2018**, *360*, 1339.

[26] M. Checa, R. Millan-Solsona, G. Gomila, *Phys. Rev. E* **2019**, *100*, 1.

[27] Q. Zhang, F. Leonardi, S. Casalini, I. Temiño, M. Mas-Torrent, *Sci. Rep.* **2016**, *6*, 1.

[28] Y. Yuan, G. Giri, A. L. Ayzner, A. P. Zoombelt, S. C. B. Mannsfeld, J. Chen, D. Nordlund, M. F. Toney, J. Huang, Z. Bao, *Nat. Commun.* **2014**, *5*, 1.

[29] S. Riera-Galindo, F. Leonardi, R. Pfattner, M. Mas-Torrent, *Adv. Mater. Technol.* **2019**, *4*, 1.

[30] A. Pérez-Rodríguez, I. Temiño, C. Ocal, M. Mas-Torrent, E. Barrena, *ACS Appl. Mater. Interfaces* **2018**, *10*, 7296.

[31] F. Leonardi, S. Casalini, Q. Zhang, S. Galindo, D. Gutiérrez, M. Mas-Torrent, *Adv. Mater.* **2016**, *28*, 10311.

[32] J. Smith, W. Zhang, R. Sougrat, K. Zhao, R. Li, D. Cha, A. Amassian, M. Heeney, I. McCulloch, T. D. Anthopoulos, *Adv. Mater.* **2012**, *24*, 2441.

[33] I. Temiño, F. G. Del Pozo, M. R. Ajayakumar, S. Galindo, J. Puigdollers, M. Mas-Torrent, *Adv. Mater. Technol.* **2016**, *1*, 1600090.

[34] M. Checa, R. Millan-Solsona, N. Blanco, E. Torrents, R. Fabregas, G. Gomila, *Nanoscale* **2019**, *11*, 20809.

[35] R. Millan-Solsona, M. Checa, L. Fumagalli, G. Gomila, *Nanoscale* **2020**, *Just*

accepted (https://doi.org/10.1039/D0NR05723A).

[36] Q. Zhang, F. Leonardi, S. Casalini, M. Mas-Torrent, *Adv. Funct. Mater.* **2017**, *27*, 1.

[37] A. . Hou, F. Ho, D. M. Bloom, **1992**, *28*, 2302.

[38] L. Fumagalli, G. Gramse, D. Esteban-Ferrer, M. A. Edwards, G. Gomila, *Appl. Phys. Lett.* **2010**, *96*, 2008.

[39] G. Gramse, G. Gomila, L. Fumagalli, *Nanotechnology* **2012**, *23*, 205703.

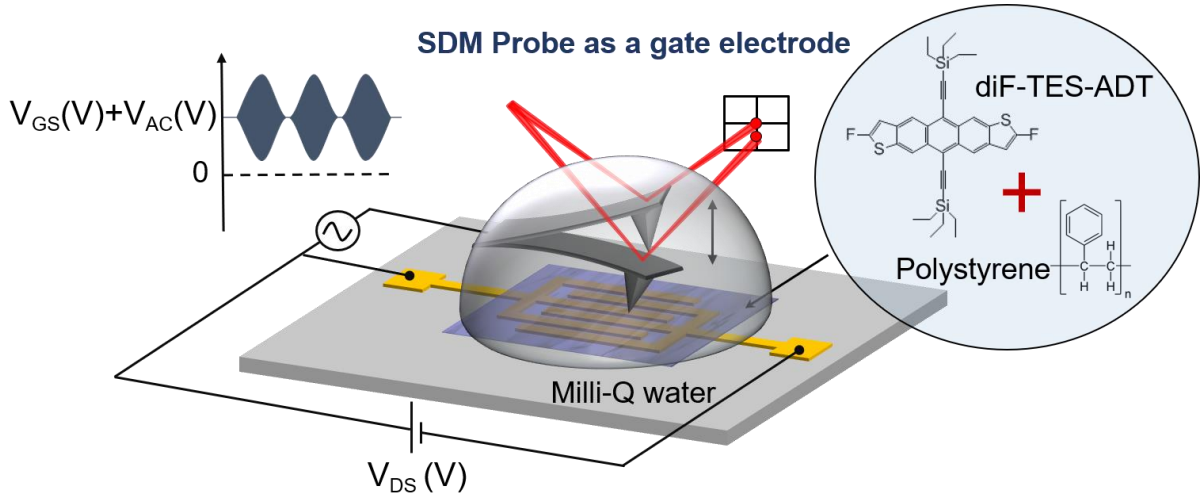

Figure 1. In-liquid SDM setup for the nanoscale electrical characterization of a functional EGOFET. An amplitude modulated AC-potential with frequency $\omega_{el} > 1$ MHz and modulation frequency ω_{mod} of about 2KHz is applied between the source of the transistor and the conductive probe in the electrolyte solution. An additional DC voltage offset is applied as a gate voltage V_{GS}. A potential V_{DS} is applied between the source and the drain, and the I_{DS} current recorded by a current-voltage source meter (not shown in the figure). The tip is scanned in the force volume mode. The SDM probe is used as both gate electrode and force sensor.

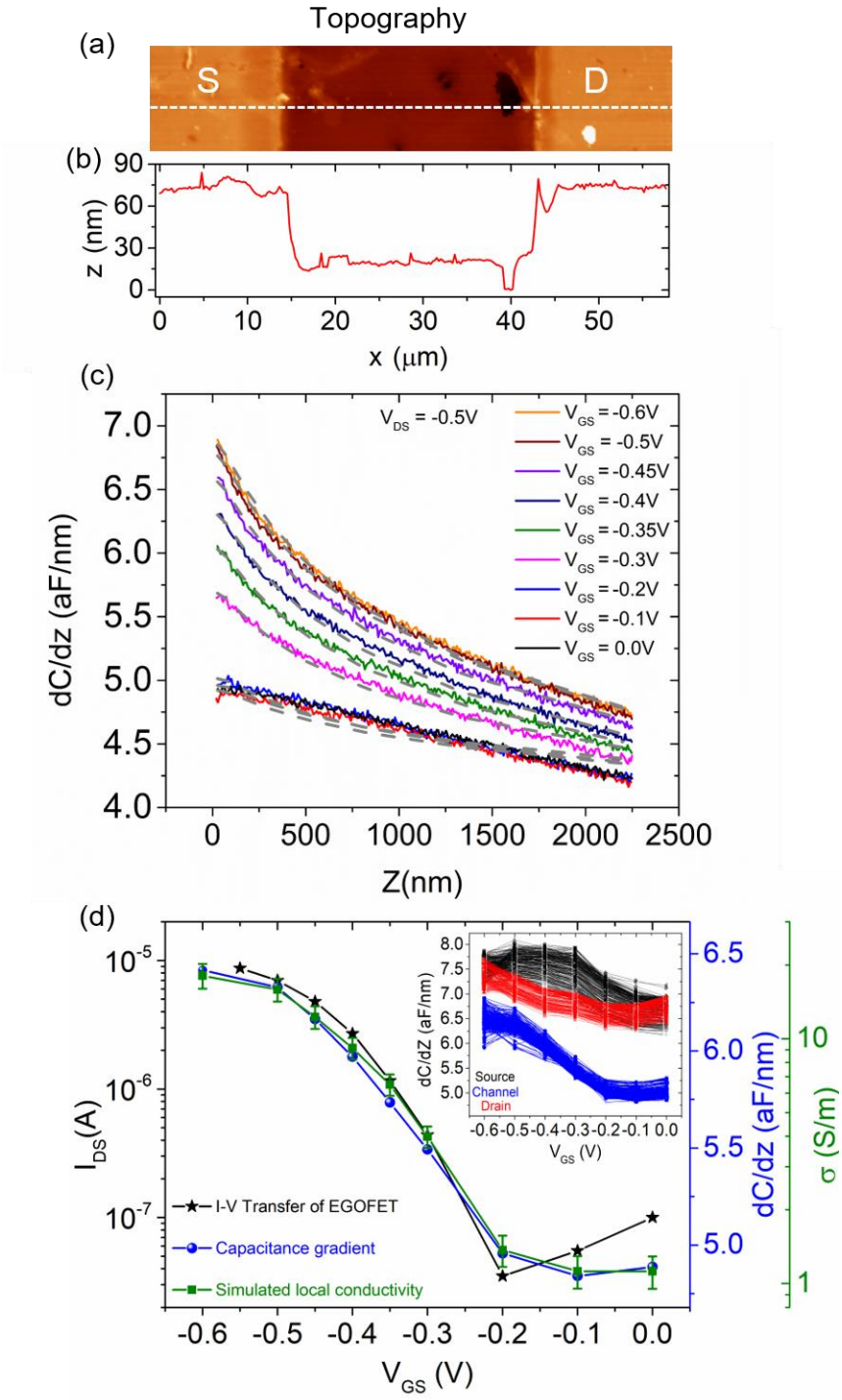

Figure 2: (a) AFM Topographic image of the semiconductor surface along the Source-Channel- Drain region of the EGOFET. (b) Topographic cross-section profile measured along the dashed line in (a). (c) Capacitance gradient (AC electric force) distance approach curves measured at the center of the transistor channel as a function of tip sample distance z at various gate voltages V_{GS} between 0 V and –0.6 V. The dashed grey lines correspond to the fitted curves to quantify the local conductivity as shown in Supporting information S5 (d) (star symbols left axis) Global current voltage transfer characteristics of the EGOFET in milliQ water measured simultaneously with an external current-voltage source meter. (blue sphere symbols right axis) AC electric force (in dC/dZ) at a distance 180 nm from the center of the channel as a function of the gate voltage V_{GS} (bottom x-axis). (Green square right y axis) Extracted local conductivity obtained by fitting the electrical curves as shown in (c). Inset:

same as the blue sphere symbols in (d) but for all points of the region shown in (a). The black, red and blue data correspond, respectively, to the source, drain and channel regions. The source drain voltage is V_{DS} =–0.5 V. Parameters used in the quantitative analysis: R=30 nm, θ=20º, H=12.5 µm, c_{int}=0.3 µF/cm^2, as obtained from electric force curves on the source at V_{GS}=–0.6 V.

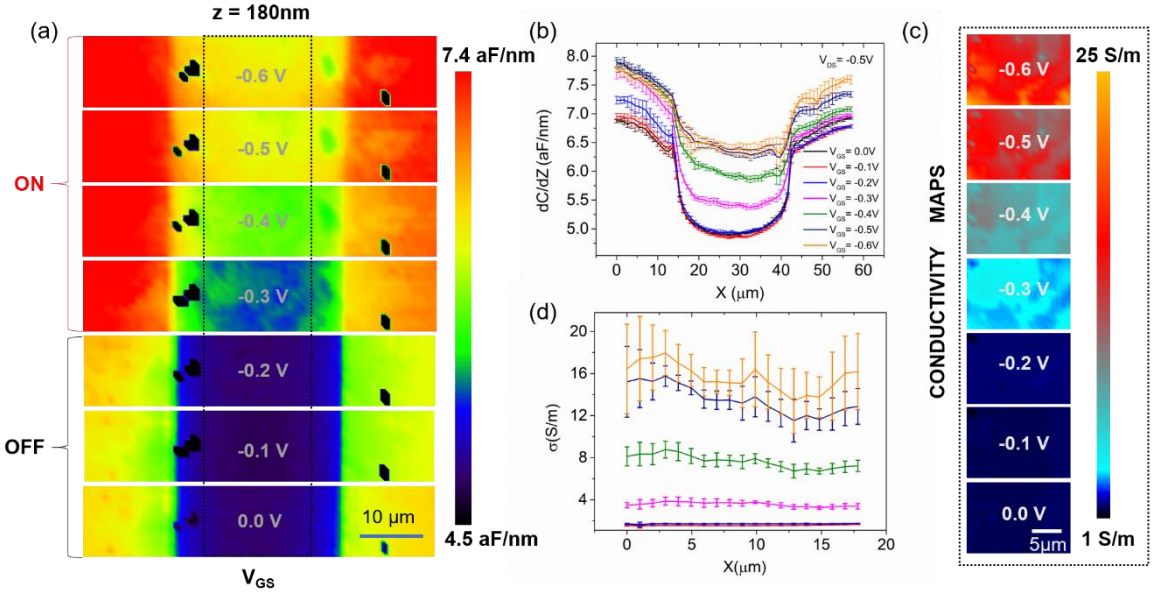

Figure 3. (a) Constant height electric force images expressed in capacitance gradient (64x13 pixels) at 180 nm from the semiconductor surface in the channel reconstructed from the electric force-voltage transfer characteristics curves shown in the inset of **Figure 2c** for various gate voltages V_{GS}. The source drain voltage was fixed at V_{DS}=–0.5 V. The dark spots represent parts of the sample whose height is above the tip height of 180 nm and whose values are not reported (we arbitrarily assigned a black colour to them). (b) Average of the 13 AC electric force cross-section profiles along the source/channel/drain in the different images in (a). (c) Conductivity maps of the central part of the channel of (a) which is obtained by a theoretical fit of each electrical curves at each pixel as in Figure 2(c) . (d) Average of the out-of-plain conductivity profiles depicting the spatial variation of the conductivity along the channel obtained from the maps in (c), by asuming a uniform interfacial capacitance as determined from measurements on the source (see Supporting Information S5).

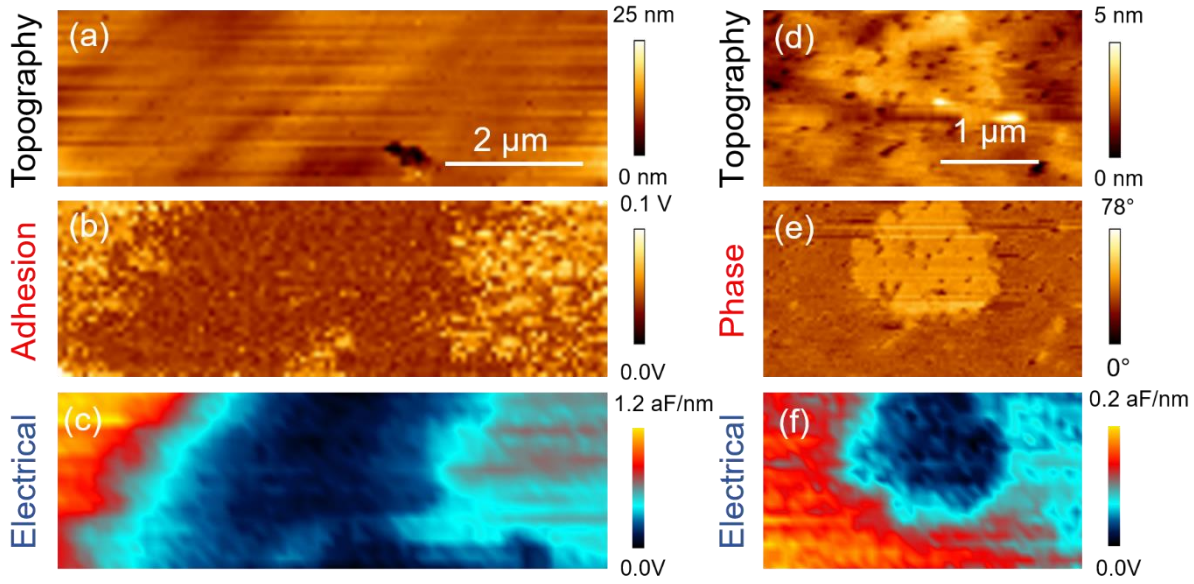

Figure 4 (a)-(c) Topographic, adhesion and constant height electric force images (128x26 pixels) of the semiconducting film on one region of the channel of the transistor in operando in milliQ water in the on state. The three images have been reconstructed from a single set of in-liquid SDM data for V_{GS}=–0.5 V, V_{DS}=–0.5 V and tip height Z=30 nm from the semiconductor surface. (d) and (e) Topographic and mechanical phase of a different region of the channel measured in intermittent contact mode. (f) Constant height electrical image (128x23 pixels) of the same region for the transistor in operando in milliQ water obtained from a set of in-liquid SDM data for V_{GS}=–0.3 V, V_{DS}=–0.5 V and tip height Z=30 nm from the semiconductor surface. Experimental in-liquid SDM parameters: modulation frequency = 2KHz, voltage amplitude= 1.5V_{PP}, electrical frequency (f = 30MHz for (c) and f = 15MHz for (f)).